Behavior of Portlandite upon Exposure to Ionizing Radiation: Evidence of Delayed H2 Production

Thibaut Herin, Thibault Charpentier, Pascal Bouniol, Sophie Le Caër

Behavior of Portlandite upon Exposure to Ionizing Radiation: Evidence of Delayed H_2 Production

Thibaut Herin[a], Thibault Charpentier[b], Pascal Bouniol,[a] and Sophie Le Caër*[b]

[a] *Université Paris-Saclay, CEA, Service de recherche en Corrosion et Comportement des Matériaux, 91191 Gif-sur-Yvette, France*

[b] *Université Paris-Saclay, CEA, CNRS, NIMBE UMR 3685, 91191 Gif-sur-Yvette, France*

**email: sophie.le-caer@cea.fr*

ABSTRACT

When used under radiation (reactor vessel well concretes, cemented radioactive waste), cementitious materials undergo radiolysis with O-H bonds leading to dihydrogen production. In order to best assess the dihydrogen (H_2) risk in nuclear facilities, it is then mandatory to check whether the solid phases of the cement matrix constitute a significant source of radiolytic H_2 in addition to that which arises from pore water. Herein, we focus on portlandite ($Ca(OH)_2$) as a main hydration product of Portland cement together with hydrated calcium silicate. In the absence of water molecules, the $Ca(OH)_2$ powder leads to an apparent H_2 radiolytic yield under accelerated electrons and γ irradiation of $(3.0 \pm 0.7) \times 10^{-9}$ mol.J^{-1} and $(8.1 \pm 0.5) \times 10^{-9}$ mol.J^{-1}, respectively. Interestingly, the H_2 production measured at the end of irradiation does not represent the whole H_2 produced; a portion of it remains trapped in the crystal lattice as evidenced by ^{1}H NMR measurements. These trapped H_2 molecules can be released after heating the sample at 453 K, leading to a total H_2 radiolytic yield for accelerated electrons and γ irradiation of $(1.1 \pm 0.2) \times 10^{-8}$ mol.J^{-1} and $(1.4 \pm 0.2) \times 10^{-8}$ mol.J^{-1}, respectively. The immediate H_2 production corresponds to the fast diffusion, if possible, of H_2 precursors to the surface with H_2 formation near or at the surface; the delayed H_2 production is due to the slow release of trapped H_2 within the material. Our work shows that the fundamental knowledge of these samples under irradiation is crucial for a better description of

materials of interest in the nuclear industry. Furthermore, the results highlight that measuring H_2 production in a solid such as portlandite is a delicate task.

INTRODUCTION

When cementitious materials are exposed to ionizing radiation due to the proximity of a radiation source (radiation shielding) or via direct contact with radioactive substances (nuclear waste embedding), safety recommendations must systematically consider the "hydrogen" risk. This risk mainly concerns the potential accumulation of H_2 in the environment (for example in storage facilities for cemented nuclear waste packages), particularly when its content exceeds 4% in the air. The release of dihydrogen (H_2) by radiolysis is generally estimated from the residual pore water stock within the material,[1–3] which thereby neglects the contribution of the solid phases. At this point, the description of radiolysis in cementitious materials seems quite complex, as it combines primary production, secondary reactions, and diffusive and convective gas transport in the pore space not occupied by water. However, various studies show that radiolytic H_2 production by the major hydrated solid phases is possible with hydrated calcium silicate (C-S-H)[4] or calcium hydroxide (portlandite, $Ca(OH)_2$)[5], or both together[6]. As the second major hydration product of Portland cement after C-S-H,[7] portlandite is differentiated by its crystallized state (microcrystals up to a few tens of micrometers)[8] and high concentration of O-H bonds (3.64×10^{22} cm^{-3}) that may play a role in the radiolysis of the solid. Unlike cementitious C-S-H, $Ca(OH)_2$ has a definite stoichiometry and is readily available as an isolated phase.

Furthermore, this hydroxide is well documented, with its $P\bar{3}m1$ structure and hexagonal symmetry, and its layered structure in the (001) plane (**Figure 1**).[9] Moreover, the structural deformations under high dose irradiation,[10] the formation of radiolytic H_2,[5,11] and the creation of radiation-induced defects[12,13] have been reported. However, in all previous irradiation studies performed on portlandite, the water content of the sample was never fully characterized nor controlled, leading to a high dispersion of the H_2 radiolytic yields reported in literature from[11] $(4.2 \pm 0.4) \times 10^{-9}$ to 2.1×10^{-8} $mol.J^{-1}$.[6] Indeed, under irradiation, water molecules are generally assumed to be more prone to H_2 production than O-H bonds.[14,15] Therefore, thermal treatment of the samples prior to irradiation decreases the H_2 radiolytic yield.[16,17] Thus, uncontrolled sorption of water

molecules can lead to an overestimation of H_2 production from O-H bonds of portlandite. Therefore, it is crucial to determine the H_2 production from ionizing radiation under strictly defined conditions, with no water molecules on the surface and as a function of different parameters of interest such as the dose rate of ionizing radiation and the particle size.

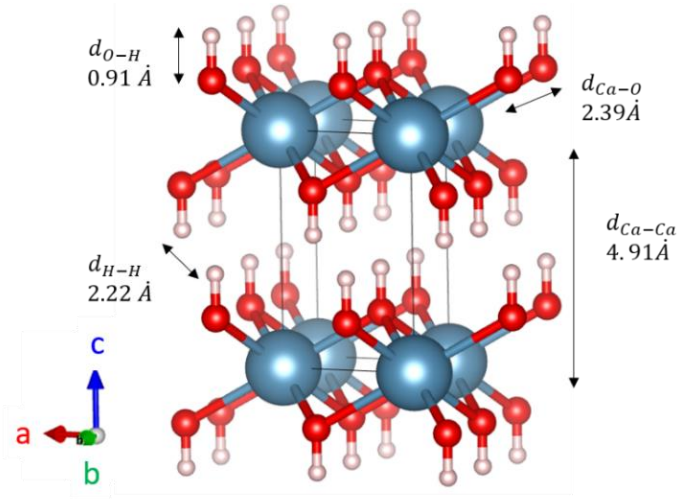

Figure 1. *Structure of $Ca(OH)_2$ and interatomic distances. Figure realized on Vesta*[18]

With this in mind, the goals of the present work are as follows: i) measure H_2 production from radiolysis of O-H bonds in $Ca(OH)_2$, ii) investigate various experimental parameters such as dose rate or surface area of portlandite, iii) understand the behavior of H_2 within this material using nuclear magnetic resonance (NMR) techniques, and iv) revisit the notion of radiolytic yield for a solid-phase, such as $Ca(OH)_2$. Great attention was paid to the preparation of the samples in order to limit as much as possible the presence of unwanted adsorbed water molecules.

METHODS

$Ca(OH)_2$ synthesis

$Ca(OH)_2$ was prepared by adding 150 mL of ultra-pure water (18.2 MΩ.cm) to CaO powder (Sigma Aldrich, 99.95%). The resulting mixture was immediately manually stirred for 2 min and filtered using a Buchner funnel with a fritted glass of porosity 4. To avoid carbonation and undesired $CaCO_3$ formation, all experiments were performed in a glove box under dinitrogen flow. To obtain a powder with a lower specific surface area,

the aforementioned powder was transferred to a hydrothermal reactor and placed into a furnace. First, the sample was heated at 373 K for 1 h. Subsequently, the temperature was increased to 513 K at a rate of 2 $K.min^{-1}$. Then, the sample was maintained at 513 K for 1 h. Lastly, the temperature was decreased to 373 K at a rate of -2 $K.min^{-1}$. This process was repeated 8 times in total.

Powder characterisation

The portlandite powder was characterized by X-ray Diffraction (XRD, **Figure S1**) and Fourier-Transform infra-red spectroscopy (FT-IR, **Figure S2**). The FT-IR spectra evidenced the presence of a minute amount of calcite ($CaCO_3$) in the sample. However, since these analyses were performed under air, calcite could have been formed during exposure to air. Moreover, thermogravimetric analysis (TGA) was performed (**Figure S3**). This measurement demonstrated that, regardless of the size of the particles, 1.8% of the calcium atoms were in the form of $CaCO_3$.

The specific surface area of both powders was measured using the BET method (**Figure S4**). The smaller particles were found to have a specific surface area of 25 $m^2.g^{-1}$, whereas the size was ten times lower (2 $m^2.g^{-1}$) for the larger particles. In addition, Dynamic Vapor Sorption (DVS) measurements (Surface Measurement Systems) were performed. Adsorption and desorption isotherms were measured on approximately 50 mg of powder placed in a small crucible. DVS was also used to measure water adsorption kinetics on dry powders. DVS experiments (**Figure S5**) showed that water adsorption on a dry sample took place in less than two minutes. Therefore, the rapid kinetics of water re-adsorption makes it impossible to expose a previously desorbed sample to air.

Transmission Electron Microscopy (TEM) experiments (**Figure S6**) were performed on the $Ca(OH)_2$ powder with the highest specific surface area. The images revealed that particles had typical sizes ranging from 50 to 100 nm. Concerning the powder with the lowest specific surface area, scanning electron microscopy (SEM) images were recorded (**Figure S7**). These images showed that most of the particles had a typical size around 1 µm, in agreement with the measured specific surface area (2 $m^2.g^{-1}$).

Sample preparation and conditioning

Irradiation of $Ca(OH)_2$ powder was performed in tightly-closed Pyrex glass ampoules of around 10.5 mL. The ampoules were filled with approximately 1000 ± 10 mg of powder.

All handling was performed in a glovebox under argon. The ampoules were subsequently filled with 1.60 bar of ultra-pure argon (99.9999%).

Thermal treatment

In order to remove sorbed water before irradiation, thermal treatment was performed on the ampoules containing the $Ca(OH)_2$ powder. TGA analysis showed that $Ca(OH)_2$ could be thermally treated up to 473-523 K without any significant modification (**Figure S3**). However, gas chromatography analysis carried out after thermal treatment evidenced that H_2 production occurred if temperature exceeded 473 K (**Figure S8**). Therefore, to remove as many water molecules as possible while avoiding thermolysis of $Ca(OH)_2$, the powders were systematically heated directly into the glass ampoules for 16 hours at 453 K under primary vacuum (2 mbar). After the thermal treatment, the ampoule was immediately filled with 1.60 bar of ultra-pure argon to ensure that the $Ca(OH)_2$ powder was never in contact with air after the thermal treatment.

$Ca(OH)_2$ irradiation

Either pulsed 10 MeV accelerated electrons or γ rays were used to irradiate the samples. In all cases, Fricke dosimetry was performed to measure the dose delivered to the sample.[19] Considering the stopping power of electrons in portlandite and in water (ESTAR program), the dose received by portlandite was considered to be, to within a few percent, the same as that received by water in the Fricke dosimeter. For electron irradiation experiments, the dose delivered by 10 ns pulses of the ALIENOR electron accelerator was 25 Gy (1 Gy = 1 $J.kg^{-1}$) per pulse, with an uncertainty of about 5%. To avoid heating of the sample, the pulse frequency was limited to 5 Hz. For the γ irradiation conditions, two different sources were employed. For lower doses, a gamma irradiator Gammacell 3000 with a ^{137}Cs source and dose rate of 4.5 $Gy.min^{-1}$ was used. For higher doses, a second irradiator with a ^{60}Co source inside a panoramic irradiation room (Institut de Chimie Physique, Orsay) was utilized. The dose rate ranged from 15 $Gy.min^{-1}$ to 45 $Gy.min^{-1}$ depending on the position of the sample in the irradiation chamber. The panoramic irradiation allowed for higher doses to be delivered to the samples that were not possible using the Gammacell. As the thickness of the portlandite sample was 1 cm, gamma photons and 10 MeV electrons passed completely through it. The dose deposited in the sample was considered to be homogeneous.

H_2 production measurement

H_2 produced after irradiation was quantified by micro-gas chromatography (μGC-R3000 SRA Instrument). Ultra-pure argon (99.9999%) was used as a carrier gas to perform the analysis. The detection limit of H_2 was 10 ppm. After each analysis, the atmosphere of the ampoule was renewed and filled with 1.6 bar of ultra-pure argon. This operation was repeated two times. To ensure reproducibility, several samples were systematically investigated.

Nuclear Magnetic Resonance (NMR) measurements

NMR experiments were performed on a Bruker Avance II Solid State NMR spectrometer operating with a magnetic field of 7.05 T (300 MHz, WB magnet). ^{1}H MAS NMR data were collected on a 4 mm (outer diameter of the ZrO_2 rotor) Bruker CPMAS probe at a spinning frequency of 12.5 kHz. Spectra were collected using the EASY pulse sequence (Elimination of Artifacts in NMR SpectroscopY)[20] for single pulse excitation spectra, and spin echo pulse sequence (90-τ-180-τ-acquisition, with τ the echo delay) with echo delays synchronized with the sample rotation. Total spectra and a spectrum recorded with minimal echo time (i.e., one rotor period) are presented in **Supporting Information S9**. Data were processed using an in-house code (T. Charpentier). Spin echo was used in order to amplify the signal of the trapped H_2 molecule. The NMR signal of the dominant (Ca)-OH species is characterized by a short T_2 time (the timescale that characterizes the decrease of the echo signal with τ) in contrast to the H_2 signal (discussed herein). Typical echo delays (synchronized with the sample rotation) were 80 μs (reference signal), 800 μs and 2 ms.

Evolution of the ^{1}H NMR spectra upon thermal treatment was investigated. With the powder still packed inside, the rotor was placed in an oven, and the cap (KelF) was removed to allow release of residual water and H_2. However, as a result, the powder was exposed to the atmosphere during this process. After each treatment, the cap on the rotor was replaced within 1 minute.

RESULTS

Unless otherwise specified, all the results are reported on the samples with the highest specific surface area.

Quantification of H_2 production under accelerated electrons irradiation

The amount of radiolytic H_2 produced by $Ca(OH)_2$ subjected to accelerated electron irradiation was measured by performing successive irradiations with steps of 40 kGy (**Figure 2a**). The amount of H_2 produced was normalized by the sample mass. The H_2 radiolytic yield (mol J^{-1}) was then obtained from the slope of the curve. The interpolation of the linear regime with the x-axis gave an apparent dose offset of 18 ± 8 kGy (**Figure 2a**). To investigate this aspect, the same experiment was performed with a dose step of 10 kGy (**Figure 2b)**. Experiments showed that when the dose was smaller than 30 kGy, the H_2 production was lower than our detection limit. Above this dose of 30 kGy, the H_2 production becomes significant (**Figure 2b**). After a short transition between 30 kGy and 60 kGy, the H_2 production was found to increase linearly with the dose beyond 60 kGy (**Figure 2b**).

Regardless of the irradiation step, the H_2 radiolytic yield $G(H_2)_{average}$ was equal to (3.0 ± 0.7) × 10^{-9} mol.J^{-1} in the linear production range. Notably, this value is smaller than those already reported in literature for experiments performed under gamma rays. For example, LaVerne and Tandon reported a radiolytic yield of 2.1 × 10^{-8} mol.J^{-1} with thermal treatment at 373 K.[5] Similarly, Acher *et al.* reported a radiolytic yield of (1.8 ± 0.4) × 10^{-8} mol.J^{-1} without thermal treatment.[11] Acher *et al.* also reported a radiolytic yield of (4.2 ± 0.4) × 10^{-9} mol.J^{-1} with thermal treatment at 423 K,[11] which is the only literature value that appears close to the value reported in our study ((3.0 ± 0.7) × 10^{-9} mol.J^{-1}) Even if the ionizing radiation is not the same (gamma rays in literature, and accelerated electrons here), the two values obtained by Acher *et al.* [11] suggests that adsorbed water was still present on the surface of portlandite, thus accounting for the high H_2 production measured. Clearly and as expected, the value of the radiolytic yield decreases when the temperature of the thermal treatment increases.

Even if the ultra-pure portlandite was available in limited amounts (starting from CaO 99.998% instead of 99.95% for the standard samples), the same irradiation protocol and H_2 measurements were applied to it. The corresponding data are given in Supporting Information (**Figure S10**). Clearly in this case, there is no dose offset, and the H_2 production is linear starting from the lowest dose, with $G(H_2)_{average}$ equal to (7.0 ± 0.7) × 10^{-9} mol.J^{-1}, i.e., a higher yield value than that measured with the less pure sample. This means that the dose offset is due to the presence of trace (metal) elements which scavenge the precursors of H_2. These trace elements, even present in limited amounts (a few tens

of ppm maximum), lead to this dose offset and lower the initial slope value by a factor of approximately 2.

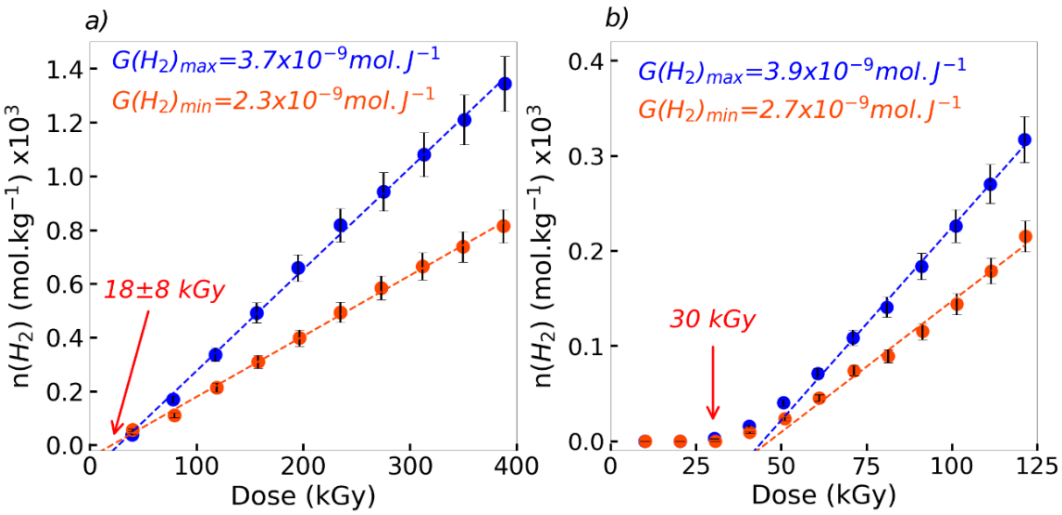

Figure 2. *H_2 radiolytic yield measured in irradiated portlandite after successive irradiations of 40 kGy (a) and 10 kGy (b). The graphs represent the cumulative H_2 production normalized by the sample weight as a function of the cumulative dose. Blue: maximum H_2 radiolytic yield obtained. Orange: minimum H_2 radiolytic yield obtained. The uncertainty on the average value (7 experiments) was estimated by computing the standard deviation of $G(H_2)$ in all experiments. The dose offset is 18 ± 8 kGy (a) while the dose at which the measurement becomes measurable is 30 kGy (b).*

The behavior of portlandite under ionizing radiation was also studied at higher doses (from a few hundreds of kGy to a few MGy, see **Figure 3**).

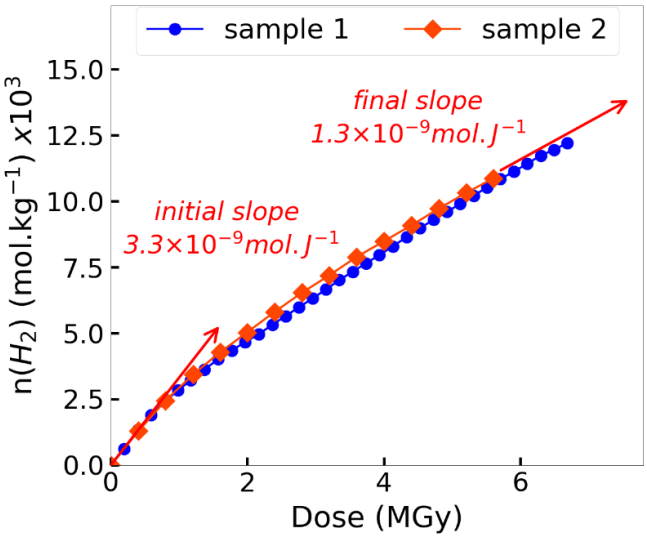

Figure 3. *H_2 production from high dose irradiated $Ca(OH)_2$ under accelerated electrons. Experiments with 200 kGy (blue) and 400 kGy (red) irradiation steps.*

At the lowest doses (Figure 3), the value of the initial slope (3.3×10^{-9} mol J^{-1}) is consistent with the H_2 radiolytic yield determined above. However, the H_2 yield decreases when the dose increases and, at the highest irradiation doses, the final value corresponds to 40% of the initial one. This behavior is attributed to a recycling mechanism (see the discussion below).

Delayed H_2 production

After irradiation, portlandite samples still produce H_2. This probably implies a slow transport of the molecule through the crystal structure. This phenomenon was also reported recently in nanostructured aluminum hydroxides (AlOOH or $Al(OH)_3$).[21,22] In order to estimate the influence of the initial dose on the delayed H_2 production, different ampoules containing the same amount of portlandite were irradiated by accelerated electrons at several doses ranging from 40 kGy to 2400 kGy. The delayed H_2 production was monitored over 2 months (**Figure 4**). Obviously, it increased with the initial dose delivered to the sample. Similarly, in boehmite (AlOOH) nanoplatelet films irradiated by electrons, the amount of desorbed H_2 after irradiation was found to increase with the electron fluence.[22] Most H_2 production was achieved within the first few days after irradiation (**Figure 4**). However, it remained significant over a period of two months after initial irradiation.

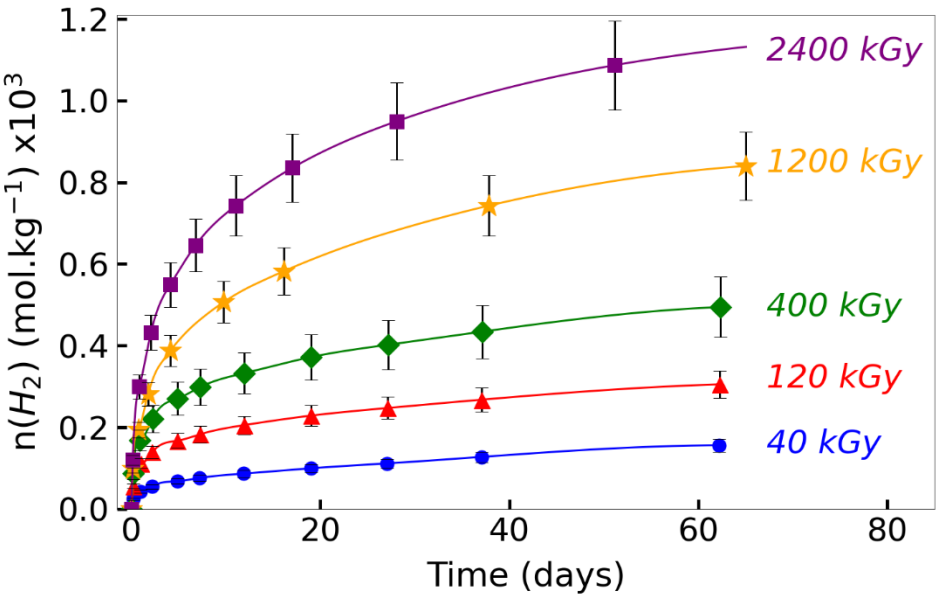

***Figure 4**. Delayed H_2 production of $Ca(OH)_2$ irradiated by accelerated electrons for different initial doses. All measurements were performed at room temperature.*

Atmosphere was renewed between each measurement. Each point takes into account the previous one, leading to a cumulative H_2 production at room temperature. Each curve corresponds to the average of two samples. Error bars are below 15%.

Moreover, the isothermal delayed H_2 production in portlandite was studied after irradiation at 320 kGy as a function of the duration of the thermal treatment for several temperatures. Firstly, three successive thermal treatments were applied to the sample (293, 348 and 398 K, see **Figure 5a**). Of course, the higher the heating temperature, the faster the delayed H_2 production kinetics and the higher the H_2 production level obtained. This behavior was also confirmed by the delayed H_2 production in samples irradiated at 400 kGy and then thermally treated at various temperatures ranging from 293 to 453 K for two months (**Figure 5b**). This latter value was chosen as the maximum temperature applied to the sample to avoid H_2 production from thermolysis (**Figure S8**). For temperatures above 373 K, the H_2 release kinetics was accelerated while the total amount of H_2 released remained globally the same. However, for temperatures below 373 K, the kinetics slowed and the H_2 released decreased as temperature decreased. In the following, we will consider that all stored H_2 is released from the irradiated samples after heating at 453 K for three days.

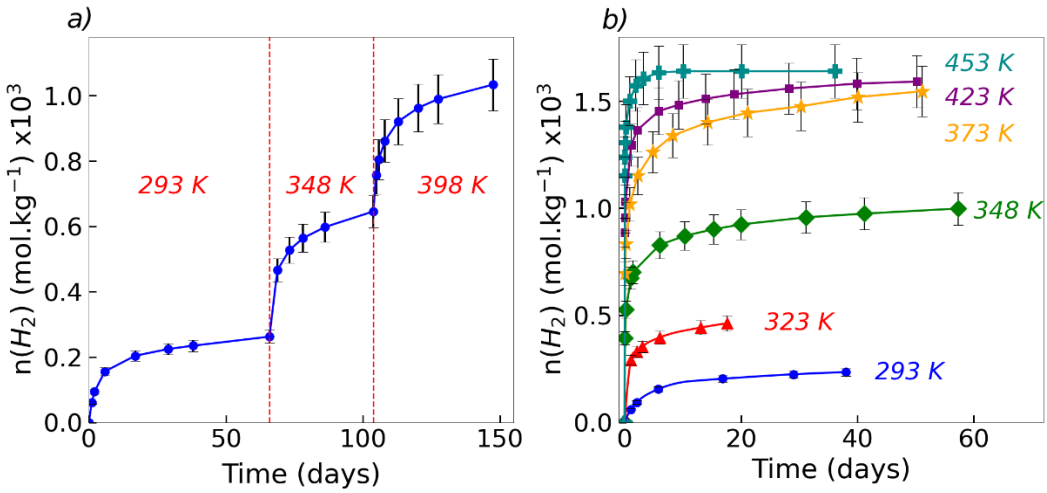

***Figure 5**. Isothermal delayed H_2 production obtained from portlandite after irradiation by accelerated electrons. a) Influence of successive heating temperatures at 293 K, 348 K and 398 K on a sample irradiated at 320 kGy. b) Influence of temperature on the delayed H_2 production on a sample irradiated at 400 kGy. In all cases, and to check reproducibility, each curve was obtained from the measurement of two samples. Note that the H_2 release kinetics could not be fitted with first or second-order models.*

Influence of specific surface area on H_2 production

Portlandite with larger particle size was also synthetized to determine the influence of the specific surface area on H_2 production (see synthesis details in the experimental section). This powder had a specific surface of 2 $m^2.g^{-1}$ (labelled as "L.S." in the following while the pristine material will be labelled as "H.S.") and a typical particle size of 1 µm (see **Figures S4b and S7**). Both immediate and delayed H_2 radiolytic yields in irradiated L.S. were determined (**Figure 6**). Evidently, the H_2 yield measured just after irradiation is lower (approximately 4 times) for the L.S. sample compared to H.S. (**Figure 6a**). A significantly lower delayed H_2 production was also observed (**Figure 6b**) with a value 9 to 10 times lower for the L.S. sample compared to H.S. one. Notably, this is approximately the same as the ratio between the specific surface area of both samples. The dose offset was also observed for large particles. The lower H_2 production of large particles made a 10 kGy step experiment impossible to precisely measure the dose offset as performed for H.S portlandite (**Figure 2b)**. As above (**Figure 2a**), the value was extrapolated from the interpolation of the linear regime with the x-axis (**Figure 6a).** An average over four experiments gave a value of 15 ± 5 kGy which is similar, within the error bars, to the value (18 ± 8 kGy) obtained for L.S. (**Figure 2a**). Again, this dose offset is due to the presence of impurities that, even if present in limited amounts, are able to scavenge the H_2 precursors.

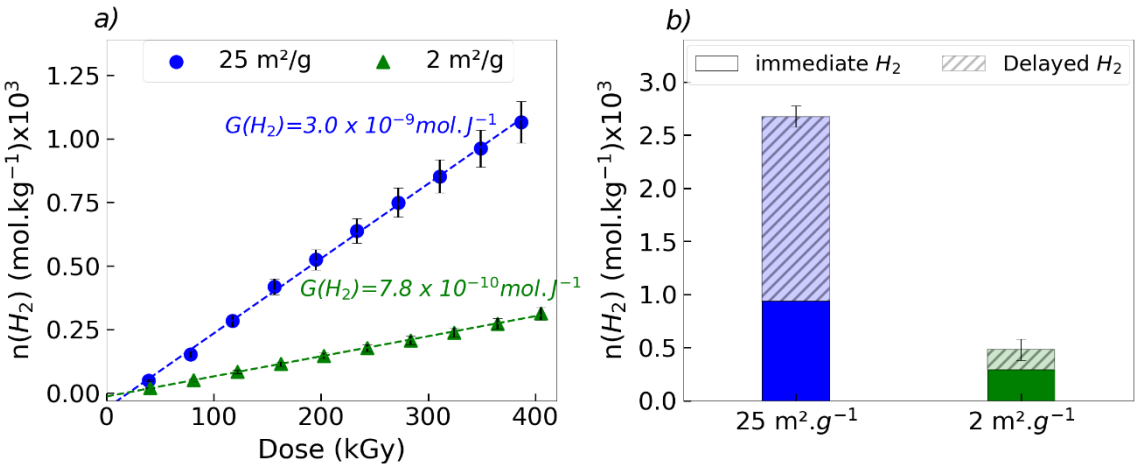

Figure 6. *Influence of the specific surface area value on the H_2 production: immediate production after irradiation with 40 kGy irradiation steps (a) and evaluation of immediate and delayed H_2 production after irradiation at a dose of 400 kGy (b). The blue color is for portlandite of 25 $m^2.g^{-1}$ of specific surface area (H.S. portlandite), and the green one for portlandite of 2 $m^2.g^{-1}$ of specific surface area (L.S. portlandite). The delayed H_2 production was measured in all cases after a thermal treatment at 453 K for three days.*

Behavior of portlandite under gamma rays

The behavior of H.S. under γ rays was also investigated. Even if γ rays and accelerated electrons have the same linear energy transfer value, γ rays provide a relatively low dose rate (continuous beam) whereas electron pulses deliver an ultra-high dose rate irradiation into the material (pulsed beam). A change of several orders of magnitude in the dose rate is well known to affect the amount of produced species in heterogeneous media.[23,24,25] It is therefore interesting to evaluate this discrepancy in H_2 production in irradiated portlandite. The shape of the H_2 production measured is very similar no matter the dose rate (see **Figure 7** and **Figure 2** for the purpose of comparison). The dose at which H_2 production becomes detectable is around 30 kGy and is similar for both irradiation conditions (see **Figure 2b**). However, in the linear part of the curve, γ irradiation led to a 2 to 3 times higher radiolytic yield than the one determined under accelerated electron irradiation (**Figure 7** as compared to **Figure 2**). Indeed, an average over 5 experiments led to $G(H_2) = (8.1 \pm 0.5) \times 10^{-9}$ mol J^{-1} under γ irradiation. Notably, gamma irradiation also led to a delayed H_2 production. Preliminary experiments evidenced that the trends were the same for both irradiation conditions: delayed production increased with the dose and a temperature increase led to faster H_2 release kinetics.

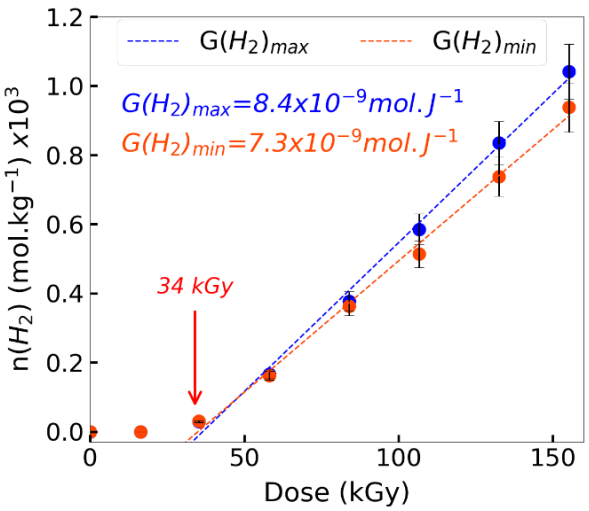

Figure 7. *H_2 radiolytic yield measurement of $Ca(OH)_2$ (H.S.) submitted to gamma rays. Blue: maximum radiolytic yield obtained; Orange: minimum radiolytic yield obtained. Measurements were performed twice a week for a dose step ranging from 15 to 20 kGy. The H_2 production becomes measurable above 34 kGy.*

The higher H_2 yield measured under γ rays than under accelerated electrons could be explained by the combination of two different reasons. Firstly, under gamma rays, each

irradiation step lasted around 3 days; comparatively, a 15-20 kGy dose is delivered to the sample in just a few minutes using accelerated electrons. This means that the H_2 measurement corresponds to the sum of the immediate H_2 production and beginning of the delayed H_2 production (**see Figure 5**) thereby increasing the values measured. Secondly, the density of created species is much larger with high dose rate irradiation (accelerated electrons) than with low dose rate (γ rays). Hence, this increases recombination reactions between electrons and holes and thus limits the formation of species, such as H_2, at a high dose rate.

^{1}H MAS NMR study of irradiated portlandite

^{1}H solid-state NMR analysis was performed on irradiated portlandite powder (H.S. sample) to follow the changes induced by irradiation in the material. A reference sample (i.e., non-irradiated) was investigated with the same experiments. The two samples were irradiated by accelerated electrons at approximately the same dose (6.5 MGy and 6.6 MGy). The Spin Echo spectra were recorded at different echo times to selectively attenuate the strong contribution of the Ca(OH) species that yield a broad signal under MAS because of the strong ^{1}H-^{1}H dipolar magnetic interactions (that are completely averaged out by MAS). But these strong interactions also cause a rapid attenuation of the signal with the echo delay. Thus, this allows species with weak couplings to the proton network to be revealed at long echo delay, thus considerably simplifying the spectra. In **Figure 8a,** spectra were recorded with the minimal echo time of 80 µs (one rotor period) to minimize the attenuation of all the signals. Under these conditions, the major contribution is due to the (Ca)O-H bonds. An echo time of 2 ms (**Figure 8b**) attenuated it almost completely. An exact interpretation of all the observed resonances beyond the scope of the present work. Hereafter, we will focus on the peaks revealed by difference between the irradiated and the non-irradiated samples. For both echo times, differences were observed between the spectra of irradiated and non-irradiated samples. The most important changes were the presence of peaks at 4.3 ppm and 0.6 ppm in the irradiated samples. The peak at 4.3 ppm can be confidently assigned to trapped H_2.[26,27] The origin of the peak at 0.6 ppm is unclear and could result from O-H bonds in an irradiation-altered environment. In the local environment of H_2, because of bond-breaking due to radiolysis, a weakening of the proton network (thus of ^{1}H-^{1}H dipolar interactions) can locally lead to species with longer T_2. This may explain the 0.6 ppm species. Interestingly, previous XRD analysis of $Ca(OH)_2$ samples irradiated at 300 MGy evidenced peaks broadening

and shift to smaller angles.[10] Although not mentioned by the authors, this result could be attributed to the deformation of the crystal due to trapped H_2 accumulation.

The influence of the thermal treatment performed on the sample was tested to compare the evolution of the peak at 4.3 ppm with the H_2 release measured by micro gas chromatography (**Figure 5**). One (reference) irradiated sample was kept at room temperature for 40 days while the other one was annealed at different successive and increasing temperatures: first at 343 K for 28 days, then at 363 K for 6 days, and finally at 388 K for 7 days. Some relevant spectra are displayed on **Figure 8c**. In what follows, we will focus on the evolution of the peak at 4.3 ppm which is characteristic of trapped H_2. Other peaks also evolve, but their assignment remains unclear and will not be discussed here. To follow the variations in the intensity of the 4.3 ppm peak, the spectrum of the non-irradiated compound was subtracted from the spectrum measured in the case of the irradiated sample (see **Figure S11** and the corresponding discussion for more details). The area of this peak is reported in **Figure 8d.** A significant decrease (about 50%) of the signal is reported during the first 28 days at 343 K. Most of this decrease took place during the 3 first days (**Figure 8d).** After 28 days at 343 K, the sample was heated at 363 K for 6 days. This led only to a small decrease of the signal intensity (**Figure 8c** & **Figure 8d)**. Annealing at 388 K afterwards induced again a decrease in the signal. Concerning the second sample kept at room temperature for 40 days (spectra not shown), only a slight decrease (5-10%) of the signal at 4.3 ppm was observed over the whole process **(Figure 8d)**. Comparison between the behavior of trapped H_2 molecules (**Figure 8d**) and the H_2 release measured by micro gas chromatography (**Figure 5**) attests to a similar behavior in both cases, evidencing that trapped H_2 molecules are then slowly released in the atmosphere (see also the discussion below).

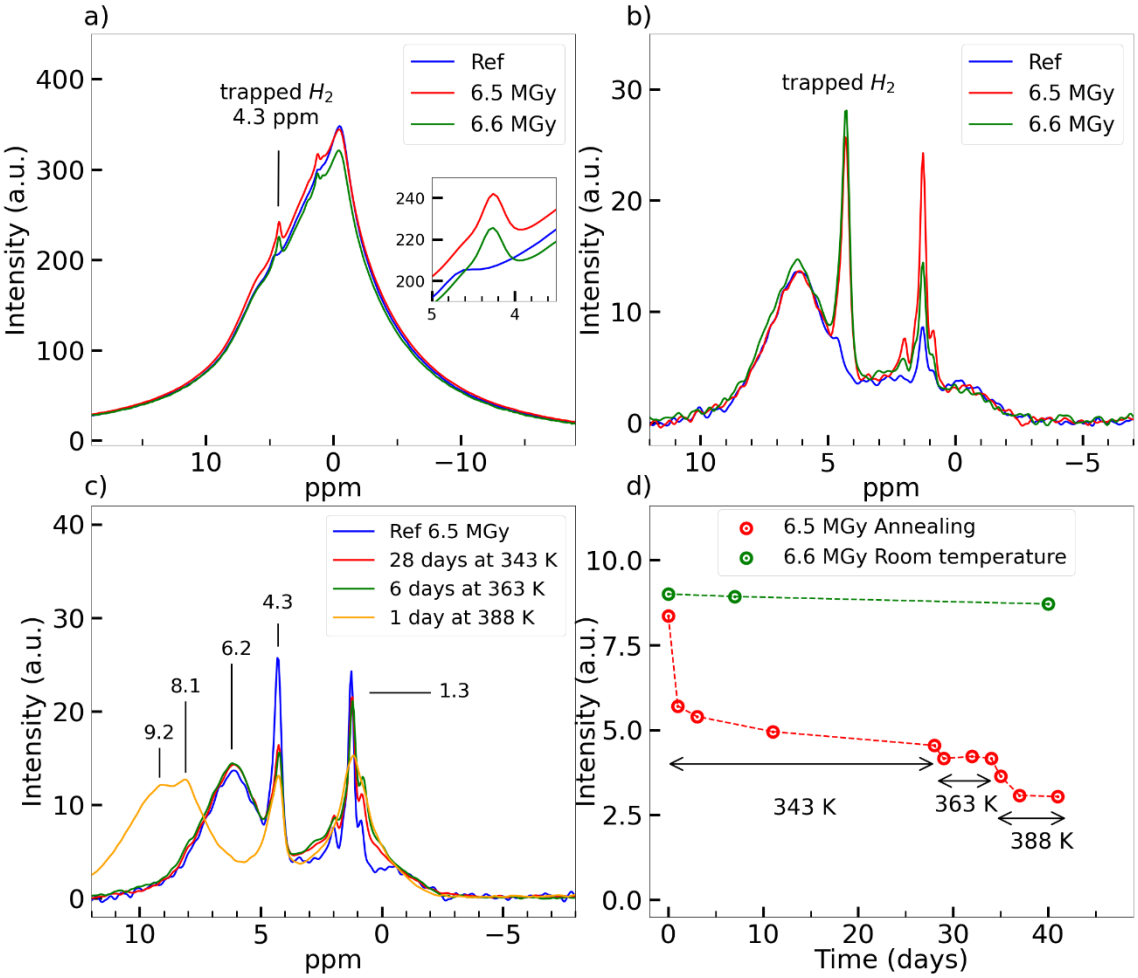

Figure 8. *^{1}H MAS NMR analysis of portlandite. a,b) Comparison of NMR spectra of irradiated (red & green) and non-irradiated portlandite (blue); a) echo time of 80 µs; b) echo time of 2 ms. c) Influence of successive annealing treatments on the NMR spectrum of portlandite irradiated at 6.5 MGy. The spectra were recorded with an echo time of 2 ms. d) Time evolution of the intensity of the 4.3 ppm peak associated to trapped H_2 at room temperature (in green), and with successive annealing temperatures (in red).*

DISCUSSION

Origin of the delayed H_2 production

H_2 is formed during irradiation, as shown by ^{1}H NMR (**Figure 8**), but must diffuse within portlandite before being released into the atmosphere. The presence of delayed H_2 is thus due to transport limitations between the bulk and the surface. Recent DFT simulations were performed on aluminum hydroxide and aluminum oxy-hydroxide to evaluate diffusion mechanisms of radiation-induced species like $H^{\bullet}$, $-O^{\bullet-}$, or H_2.[28] The authors have shown that the energy barriers for $H^{\bullet}$ and H_2 diffusion are high (well above thermal energy), which accounted for the presence of trapped H_2 in boehmite (γ-AlOOH).[21] A similar result can be expected for portlandite. However, this delayed H_2

release is not entirely consistent with a Fick's diffusion of trapped molecular H_2. Indeed, the increase in temperature should only lead to an increase in the rate constant of H_2 release without changing the amount released. Such behavior was not observed for temperatures below 373 K (**Figure 5b**). One explanation could be that trapped H_2 is present in several trapping environments. Each trapping site requires a different de-trapping temperature, inducing a H_2 release by steps, if the temperature is not high enough. In this case, the peak at 4.3 ppm detected by NMR and assigned to trapped H_2 (**Figure 8**) could be composed of several peaks too close to be distinguished. Another explanation could also be that H_2 diffusion does not follow Fick's relation creating a sub-diffusive process.

To support the hypothesis of a delayed production due to trapped molecular H_2 diffusion, the evolution of the signal at 4.3 ppm (**Figure 8d)** can be compared to the delayed H_2 release given in **Figure 5a**. Indeed, a similar behavior between both experiments is found. First, the small decrease of the signal at 4.3 ppm at room temperature is consistent with a possible but limited delayed H_2 production for such temperature. The decrease of around 50% of the 4.3 ppm peak intensity at 343 K (**Figure 8d)** is consistent with the first H_2 production plateau evidenced at 348 K in **Figure 5a**. In both experiments, this temperature was not high enough to release all H_2 molecules trapped inside the solid. Increasing the temperature to 363 K, even if accelerating slightly the decrease, was likely still not sufficient to induce massive H_2 de-trapping. Treatment at 388 K caused the 4.3 ppm signal to decrease again in a few days. Regarding the results of **Figure 5b**, this temperature is high enough to fully release the trapped H_2, but a longer time would have been necessary to allow the whole release. These experiments prove that a certain amount of H_2 is trapped in the material, that it is responsible for the observed delayed production and that heating is necessary to release it even if a slight production a is possible at room temperature.

Of course, other reactions could account for the delayed H_2 production. For instance, $H^{\bullet}$ atoms trapped in the material could slowly dimerize into H_2. However, Electron Paramagnetic Resonance (EPR) spectra measured at room temperature do not evidence the presence of any $H^{\bullet}$ atom (data not shown) contrary to boehmite (AlOOH)[29] or talc (a clay mineral[30]) for which trapped $H^{\bullet}$ atoms were found at room temperature. In the case of boehmite, hydrogen atoms were suggested to be trapped in cavities between interstitial layers;[29] likewise, for talc,[30] it was suggested that hydrogen atoms were trapped in the

octahedral sheet and protected by two adjacent tetrahedral sheets. This is not the case in portlandite. Therefore, we can conclude that the delayed H_2 production is due to trapped H_2 in the material, the diffusion of which appears limited in the crystal lattice.

Evolution of immediate and delayed H_2 production

Because of the presence of delayed H_2, the H_2 production resulting from $Ca(OH)_2$ irradiation is difficult to quantify exactly. As explained above, a heat treatment at 453 K for three days was applied to release trapped H_2 from the irradiated samples. The amount of H_2 released during this treatment was called $n_{delayed}$ while $n_{immediate}$ was defined as the H_2 amount directly measurable after irradiation. n_{tot} is then defined as the sum of these two terms:

$$n_{tot} = n_{immediate} + n_{delayed} \qquad \text{(Eq 1)}$$

n_{tot} is useful for tracing the actual yield resulting from the primary event (O-H bond cleavage) and the subsequent reaction mechanism (H_2 formation, recombination reactions, see below), $n_{immediate}$ is useful to trace the apparent yield for operational purposes. The evolution of n_{tot} (normalized by the sample mass) and of its two components $n_{immediate}$ and $n_{delayed}$ as a function of the dose was studied under accelerated electron irradiation for doses ranging from 10 kGy to 5.7 MGy (**Figure 9a)**. In addition, the proportion of each contribution to the total H_2 is represented in **Figure 9b**. Note that in **Figures 2 and 3**, only the immediate production was determined. Obviously, when the dose is as low as 10 kGy, only delayed H_2 is detected (**Figure 9b**) and no immediate H_2 which is consistent with the dose offset observed in **Figure 2**. H_2 is thus mainly stored within the material for low doses. An effective radiolytic yield defined as the derivative of the production curve of each quantity was numerically computed **in Figure S12**.

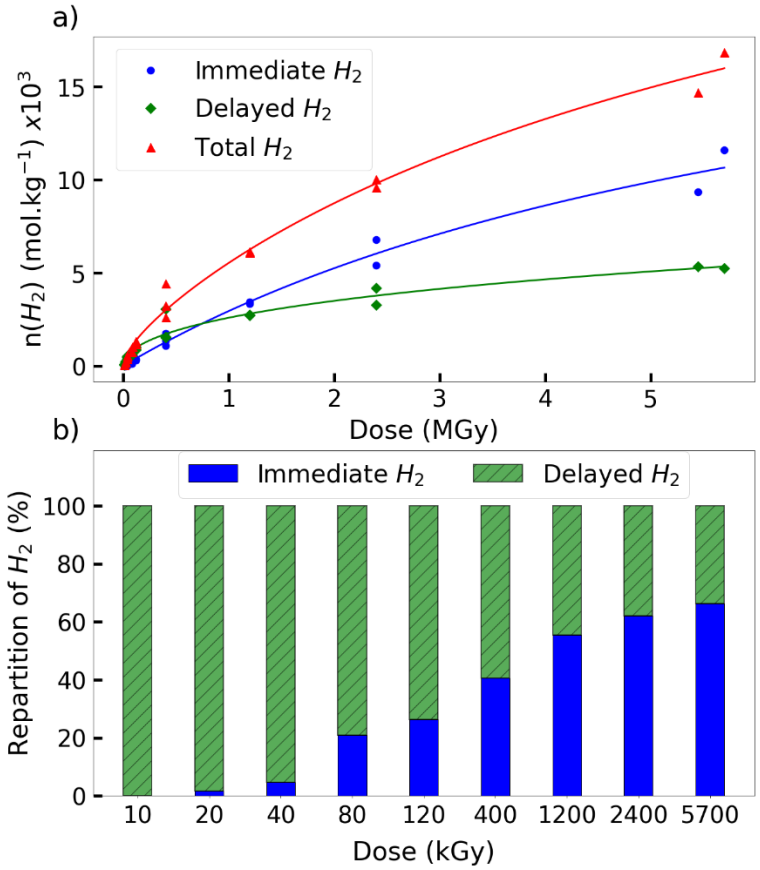

Figure 9. *a) Evolution of the amounts of "immediate" (blue), "delayed" (green) and total H_2 (red) normalized by the sample mass for different doses under accelerated electrons irradiation. The lines correspond to fits of the data. b) Contribution of the immediate and delayed H_2 production to the total one for the different doses. Each point represents a single irradiation performed on an independent sample. For each dose, at least two samples were irradiated and heated in order to ensure reproducibility of the results.*

After several MGy, the decrease of the immediate production for the one-shot irradiation **(Figure 9a)** is consistent with the decrease already reported for successive irradiations (**Figure 3**). The same trend –even more pronounced– is also observed for delayed H_2 **(Figure 9b)**. It represents 100% of the total H_2 at 10 kGy and only 34% at 5.7 MGy. This suggests that an *in situ* consumption of H_2 or its precursors occurs which is all the more efficient as the dose increases (see discussion below).

Evolution of n_{tot} was also studied under gamma irradiation (**Figure 10**). Due to the low dose rate, only doses ranging from 0 kGy to 160 kGy could be explored. Data corresponding to accelerated electron irradiation and belonging to this dose range are also added to the graph for the purpose of comparison. Clearly, n_{tot} evolves linearly with the dose in the dose range considered. The slope of the line, i.e., the total H_2 radiolytic yield, is slightly higher (25%) for gamma irradiation (1.4×10^{-8} mol J^{-1}) than for accelerated

electrons (1.1×10^{-8} mol J^{-1}). Such a difference could be explained by a dose rate effect inducing a total H_2 production slightly higher for gamma rays than for accelerated electrons. Indeed, as stated above, the density of created species is much larger with high dose rate irradiation (accelerated electrons) than with the low dose rate irradiation (gamma rays). Therefore, this increases recombination reactions between electrons and holes and limits the formation of H_2 at a high dose rate.

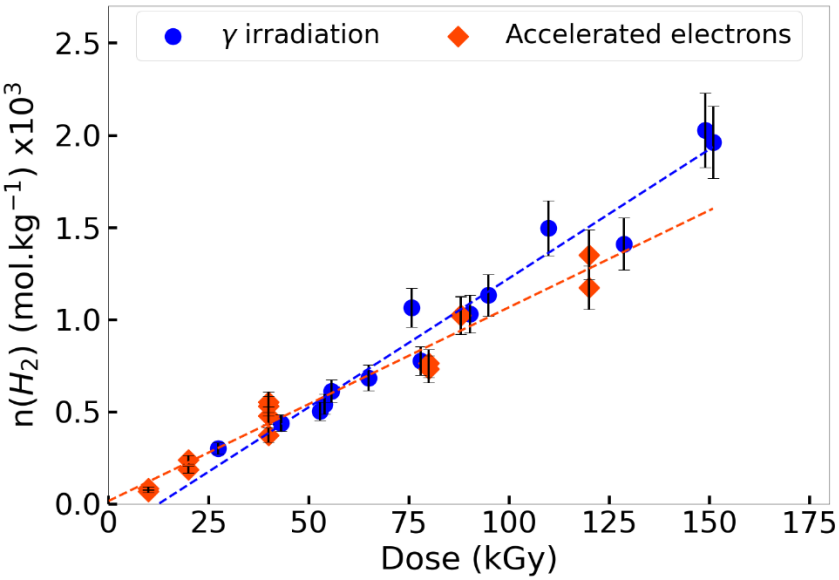

***Figure 10**. Evolution of the total H_2 amount with the dose. Blue circles: gamma irradiation with ^{60}Co source. Red diamonds: accelerated electrons irradiation. Each point represents an independent sample. The slope of the line, i.e., the total H_2 radiolytic yield, is (1.4×10^{-8} mol J^{-1}) under gamma irradiation and (1.1×10^{-8} mol J^{-1}) under accelerated electrons irradiation.*

Even if the total amount of produced H_2 is globally the same for both types of experiments, the distribution between immediate and delayed H_2 differs due to dose rate effects. Indeed, the immediate production of H_2 under gamma irradiation was found to be almost 2.6 times higher than under accelerated electrons (**Figure 2b** vs **Figure 7**). As gamma irradiations are performed over several days whereas electron irradiations require a few hours at maximum, delayed production occurred simultaneously with immediate production. However, and especially at room temperature, the delayed production alone could not explain this 2.6-fold increase. A dose rate effect may thus account for this.

Influence of various parameters (dose rate, size effect) on partial H_2 recycling

To account for the charge repartition, the metallic cation Ca (Ca^{2+} in fact) is considered to be bound with hydroxyl groups OH^- composed by an anionic oxygen O^{2-} and a H^+ proton.

Upon ionizing radiation, electron-hole pairs (R1), as well as excitons, are formed in portlandite.

$Ca(OH)_2 \rightsquigarrow h^+ + e^-$ (R1)

The h^+ hole can then become trapped the oxygen atom, leading to the release of a proton (R2).

$\equiv CaOH^- + h^+ \rightarrow \equiv CaO^{\bullet -} + H^+$ (R2)

The electron may react with a proton, leading to the formation of a hydrogen atom (R3), or undergo a dissociative attachment on –OH groups (R4).

$H^+ + e^- \rightarrow H^\bullet$ (R3)

$\equiv CaOH^- + e^- \rightarrow \equiv CaO^{2-} + H^\bullet$ (R4)

The excitons may also react with $\equiv CaOH^-$, leading then to the formation of $\equiv CaO^{\bullet -}$ and of $H^\bullet$ atoms.

Then, the very reactive $H^\bullet$ atoms dimerize to form H_2 (R5):

$H^\bullet + H^\bullet \rightarrow H_2$ (R5)

It can also abstract one hydrogen atom from $\equiv CaOH^-$ to form H_2 (R6):

$\equiv CaOH^- + H^\bullet \rightarrow \equiv CaO^{\bullet -} + H_2$ (R6)

Various reactions are also given in section 13 of the Supporting Information.

The electron, the hydrogen atom, the exciton and the H^+ ion are mobile species that can be transferred to the surface of portlandite to lead to immediate H_2 production. The observed dose offset is just the result of the trapping of these precursors by impurities present in the sample. Of course, these species can also produce *in situ* H_2 that will then be trapped in the material and will be released progressively. If H_2 is produced near the surface, then it will contribute to the immediate production.

One may also wonder why the H_2 production is lower at high doses. This is especially true for the delayed H_2 release (**Figures 3 and 9**). A quick evaluation shows that depletion of O-H bonds is not responsible for this trend. Indeed, if we crudely consider a H_2 radiolytic yield of 3.3×10^{-9} mol J^{-1} for a total dose of 6 MGy, then 1.98×10^{-2} mol(H_2) are produced per kg of sample, i.e., 3.96×10^{-2} mol(H) per kg. This means that

approximately 0.15% of the O-H bonds available in portlandite are affected by ionizing radiation at this high dose. Even if this number reaches 0.3% by considering that around 50% of the total H_2 is stored within the material, it is negligible. This proves that the decrease of intact O-H bonds in the material upon irradiation cannot account for this trend. Therefore, the decrease of H_2 production is attributed to a recycling mechanism. A crude simulation, based on six reactions was performed (**Figures S13 and S14** and associated discussion). It reproduces the total H_2 production from 10 kGy to 5.7 MGy (**Figure 9a**). In this simulation, the H_2 recycling was due to the recycling of its precursor (the hydrogen atom in the simulation performed, see section 13 in the Supporting Information). However, the behavior of the sample under irradiation is rather complex, and it is likely that other simulations could lead to a satisfying fit with a recycling of H_2 itself. The recycling also accounts for the results obtained by changing the dose rate or the size of the portlandite crystals.

As discussed above, the delayed production of H_2 is due to the slow diffusion of this molecule across the crystal lattice. With larger particles, the average path of H_2 or of its precursors to the surface is longer, therefore increasing recycling processes. The larger distances lead also to a higher residence time of the highly reactive species, inducing a better recycling process in the larger particles. Both factors account for a decreased H_2 production, whether immediate or delayed, in the larger particles as compared to the smaller ones. Interestingly, a factor of 2 was measured between the size of the Scherrer domains measured by XRD (**Figure S1**) between H.S. and L.S. This corresponds to a factor of four between the two samples when considering the area belonging to the crystallized domains. The immediate production could then be the result of a surface effect produced by highly mobile species that move into the crystallized domains and form H_2 on the surface of the particles, or very close to the surface.

Recycling also accounts for the differences measured in the delayed H_2 production under γ and accelerated electrons. Indeed, in the H.S. sample the apparent H_2 radiolytic yield is $(3.0 \pm 0.7) \times 10^{-9}$ mol.J^{-1} and $(8.1 \pm 0.5) \times 10^{-9}$ mol.J^{-1} under accelerated electrons and γ irradiation respectively. Comparatively, the total H_2 radiolytic yield $G(H_2)_{tot}$ is equal to $(1.1 \pm 0.2) \times 10^{-8}$ mol.J^{-1} and $(1.4 \pm 0.2) \times 10^{-8}$ mol.J^{-1} for accelerated electrons and γ irradiation respectively. This means that the H_2 delayed yield is higher for an irradiation performed under accelerated electrons (8.0×10^{-9} mol.J^{-1}, high dose rate irradiation) that under γ rays (5.9×10^{-9} mol.J^{-1}, low dose rate irradiation). Under a high dose rate

irradiation, more recombination reactions certainly lead to fewer defects accumulation, and hence, to less recycling processes, leading to an increased H_2 accumulation in the particles.

CONCLUSIONS

The behavior under irradiation of portlandite, a major hydration product of Portland cement, was investigated. It is a radiolysable solid whose behavior under irradiation was shown to be complex. The H_2 yields measured immediately after irradiation were on the order of 3×10^{-9} mol J^{-1} and 8×10^{-9} mol J^{-1} for accelerated electrons and γ irradiation, respectively. These values are approximately one order of magnitude lower than the one obtained in bulk water (4.8×10^{-8} mol J^{-1}). Our results also show the very important role played by trace elements present in very small quantities for H_2 production and its behavior with dose. Moreover, the yields measured are underestimated because a part of the H_2 formed *in situ* remains stored within the $Ca(OH)_2$ structure. As the diffusion of H_2 is limited in the crystal lattice, the H_2 production shows a delayed component related to its slow migration kinetics to the surface of the sample. However, the delayed release of H_2 as a function of temperature is not consistent with a pure diffusive model, which would suggest the existence of different trapping sites for H_2 molecules. The total radiolytic H_2 yield, defined as the sum of immediately measurable and delayed production, is equal to 1.1×10^{-8} mol J^{-1} and 1.4×10^{-8} mol J^{-1} for accelerated electrons and gamma, respectively. The slightly higher value measured in the second case could be due to less efficient recombination reactions due to a much lower dose rate.

The immediate H_2 production is related to the fast diffusion, if possible, of H_2 precursors to the surface and H_2 formation near or at the surface. The delayed production corresponds to the slow release of trapped H_2 within the material. The existence of immediate and delayed H_2 results then from the coupling between diffusive transport and *in situ* recombination reactions. The relative importance of transport and recombination reactions is modified by particle size (species residence time) and dose rate (event density).

These results enable better understanding of the behavior of a major constituent of cementitious materials used in the context of nuclear applications, in particular the cementation of radioactive waste. Taking into account our results, a better modelling of

H_2 produced by nuclear waste is expected. However, they need to be complemented by the properties of the cementitious C-S-H in order to know the overall behavior of the cement paste under irradiation.

ASSOCIATED CONTENT

Supported information

X-Ray Diffraction (XRD) analysis of $Ca(OH)_2$; Fourier Transform Infrared Spectroscopy (FT-IR); thermogravimetric analysis (TGA); BET analysis; Dynamic Vapor Sorption (DVS) analysis; TEM images; SEM images; thermolysis of $Ca(OH)_2$; NMR spectra of $Ca(OH)_2$; H_2 production in ultra-pure portlandite samples; decomposition of NMR spectra; effective radiolytic yield; partial H_2 recycling.

ACKNOWLEDGMENTS

EDF and CEA are gratefully acknowledged for financial support. Jorge Vieira is gratefully acknowledged for his help during the experiments with the linear accelerator ALIENOR. The authors thank Frédéric Gobeaux for the microscopy experiments, Alexandre Demarque for the gamma irradiations at Institut de Chimie Physique, Université Paris Saclay, Emilie Thory for the BET measurements and Stéphane Poyet for the sorption balance experiment. Taren Cataldo is gratefully acknowledged for his careful reading of the manuscript.

REFERENCES

(1) Bouniol, P.; Bjergbakke, E. A Comprehensive Model to Describe Radiolytic Processes in Cement Medium. *J. Nucl. Mater.* **2008**, *372*, 1–15.

(2) Foct, F.; Di Giandomenico, M.-V.; Bouniol, P. Modelling of Hydrogen Production from Pore Water Radiolysis in Cemented Intermediate Level Waste. In *EPJ Web of Conferences*; 2013; pp 1-1–8.

(3) Offermann, P. Calculation of the Radiolytic Gas Production in Cemented Waste. *Mater. Res. Soc.* **1988**, *127*, 461–469.

(4) Yin, C.; Dannoux-Papin, A.; Haas, J.; Renault, J. P. Influence of Calcium to Silica Ratio on H_2 Gas Production in Calcium Silicate Hydrate. *Radiat. Phys. Chem.* **2019**, *162*, 66–71.

(5) LaVerne, J. A.; Tandon, L. H_2 and Cl_2 Production in the Radiolysis of Calcium and Magnesium Chlorides and Hydroxides. *J. Phys. Chem. A* **2005**, *109*, 2861–2865.

(6) Bouniol, P. Contribution of the Tricalcium Silicate Hydration Products to the Formation of Radiolytic H_2: A Systemic Approach. *J. Adv. Concr. Technol.* **2022**, *20*, 72–84.

(7) Richardson, I. G. The Nature of the Hydration Products in Hardened Cement Pastes. *Cem. Concr. Compos.* **2000**, *22*, 97–113.

(8) Diamond, S. The Microstructure of Cement Paste and Concrete — a Visual Primer. *Cem. Concr. Compos.* **2004**, *26*, 919–933.

(9) Busing, W. R.; Levy, H. A. Neutron Diffraction Study of Calcium Hydroxide. *J. Chem. Phys.* **1957**, *26*, 563–568.

(10) Noirfontaine, D.; Acher, L.; Courtial, M. An X-Ray Powder Diffraction Study of Damage Produced in $Ca(OH)_2$ and $Mg(OH)_2$ by Electron Irradiation Using the 2.5 MeV SIRIUS Accelerator. *J. Nucl. Mater.* **2018**, *509*, 78–93.

(11) Acher, L.; Chartier, D.; Haas, J.; Courtial, M.; Dunstetter, F.; Tusseau-Nenez, S. Radioactive Waste Conditioning: The Choice of the Cement Matrix versus Irradiation, Paper Number 029 In *37th Cement and Concrete Science Conference*, London, United Kingdom, Sept 11-12, **2017**.

(12) Barsova, L.I.; Yurik, T.K.; Spitsyn, V. I. Radiation Centers in Alkaline-Earth Hydroxides. *Bull. Acad. Sci. USSR*, **1986**, *35*, 969–974.

(13) Spitsyn, V. I.; Yurik, T.K.; Barsova, L.I.. Atomic Hydrogen in Gamma-Irradiated Hydroxides of Alkaline-Earth Elements. *URSS Chem Bull* **1982**, *31*, 672–677.

(14) Brodie-Linder, N.; Le Caer, S.; Renault, J. P.; Alba-Simionesco, C. H_2 Formation by Electron Irradiation of SBA-15 Materials and the Effect of Cu^{II} Grafting W. *Phys. Chem. Chem. Phys.* **2010**, *12*, 14188–14195.

(15) Shcherbakov, V.; Charpentier, T.; Denisov, S.; Mostafavi, M.; Thill, A. Confined Water Radiolysis in Aluminosilicate Nanotubes: The Importance of Charge Separation Effect. *Nanoscale* **2021**, *13*, 3092–3105.

(16) Petrik, N. G.; Alexandrov, A. B.; Vall, A. I. Interfacial Energy Transfer during

Gamma Radiolysis of Water on the Surface of ZrO_2 and Some Other Oxides. *J. Phys. Chem. B* **2001**, *105*, 5935–5944.

(17) Acher, L. Etude Du Comportement Sous Irradiation γ et Électronique de Matrices Cimentaires et de Leurs Hydrates Constitutifs, PhD thesis of Paris-Saclay University, **2018**.

(18) Momma, K.; Izumi, F. VESTA 3 for Three-Dimensional Visualization of Crystal, Volumetric and Morphology Data. *J. Appl. Crystallogr.* **2011**, *44*, 1272–1276.

(19) Fricke, H.; Hart, J. E. In *Radiation Dosimetry, 2nd Ed.;* Attix, F.H., Roesch, W.C., Eds.; Academic Press: New York, **1966**; p. 167-232.

(20) Jaeger, C.; Hemmann, F. EASY: A Simple Tool for Simultaneously Removing Background, Deadtime and Acoustic Ringing in Quantitative NMR Spectroscopy - Part I: Basic Principle and Applications. *Solid State Nucl. Magn. Reson.* **2014**, *57–58*, 22–28.

(21) Kaddissy, J. A.; Esnouf, S.; Durand, D.; Saffre, D.; Foy, E.; Renault, J. P. Radiolytic Events in Nanostructured Aluminum Hydroxides. *J. Phys. Chem. C* **2017**, *121*, 6365–6373.

(22) Jones, B. M.; Aleksandrov, A. B.; Zhang, X.; Rosso, K. M.; LaVerne, J. A.; Orlando, T. M. Electron-Stimulated Formation and Release of Molecular Hydrogen and Oxygen from Boehmite Nanoplatelet Films. *J. Phys. Chem. C* **2022**, *126*, 2542–2547.

(23) Blain, G.; Vandenborre, J.; Fiegel, V.; Fois, R.; Haddad, F.; Koumeir, C.; Maigne, L.; Me, V.; Poirier, F.; Potiron, V.; Poirier, F. Proton Irradiations at Ultra-High Dose Rate vs . Conventional Dose Rate : Strong Impact on Hydrogen Peroxide Yield. *Rad. Res.* **2022**, *198*, 318–324.

(24) Rotureau, P.; Renault, J. P.; Lebeau, B.; Patarin, J.; Mialocq, J. Radiolysis of Confined Water : Molecular Hydrogen Formation. *ChemPhysChem* **2005**, *6*, 1316–1323.

(25) Le Caër, S.; Rotureau, P.; Brunet, F.; Charpentier, T.; Blain, G.; Renault, P.; Mialocq, J. Radiolysis of Confined Water : Hydrogen Production at a High Dose Rate. *ChemPhysChem* **2005**, *6*, 2585–2596.

(26) Fujiwara, H.; Yamabe, J.; Nishimura, S. Determination of Chemical Shift of Gas-Phase Hydrogen Molecules by 1H Nuclear Magnetic Resonance. *Chem. Phys. Lett.* **2010**, *498*, 42–44.

(27) Senadheera, L.; Carl, E. M.; Ivancic, T. M.; Conradi, M. S.; Bowman, R. C.; Hwang, S. J.; Udovic, T. J. Molecular H_2 Trapped in AlH_3 Solid. *J. Alloys Compd.* **2008**, *463*, 1–5.

(28) Shen, Z.; Ilton, E. S.; Prange, M. P.; Mundy, C. J.; Kerisit, S. N. Diffusion Mechanisms of Radiolytic Species in Irradiated Al (Oxy-)Hydroxides. *J. Phys. Chem. C* **2018**, *122*, 28990–28997.

(29) Laverne, J. A.; Huestis, P. L. H Atom Production and Reaction in the Gamma Radiolysis of Thermally Modified Boehmite. *J. Phys. Chem. C* **2019**, *123*, 21005–21010.

(30) Lainé, M.; Allard, T.; Balan, E.; Martin, F.; Von Bardeleben, H. J.; Robert, J. L.; Le Caër, S. Reaction Mechanisms in Talc under Ionizing Radiation: Evidence of a High Stability of H• Atoms. *J. Phys. Chem. C* **2016**, *120*, 2087–2095.

Graphical abstract